

Near- and long-term quantum algorithmic approaches for vibrational spectroscopy

Nicolas P. D. Sawaya,^{1,*} Francesco Paesani,^{2,3,4} and Daniel P. Tabor^{5,†}

¹*Intel Labs, Santa Clara, CA 95054, USA*

²*Department of Chemistry and Biochemistry,
University of California San Diego, La Jolla, CA 92093, USA*

³*Materials Science and Engineering,
University of California San Diego, La Jolla, CA 92093, USA*

⁴*San Diego Supercomputer Center, University of
California San Diego, La Jolla, CA 92093, USA*

⁵*Department of Chemistry, Texas A&M University, College Station, TX 77843, USA*

(Dated: September 14, 2020)

Abstract

Determining the vibrational structure of a molecule is central to fundamental applications in several areas, from atmospheric science to catalysis, fuel combustion modelling, biochemical imaging, and astrochemistry. However, when significant anharmonicity and mode coupling are present, the problem is classically intractable for a molecule of just a few atoms. Here, we outline a set of quantum algorithmic methods for solving the molecular vibrational structure problem for both near- and long-term quantum computers. There are previously unaddressed characteristics of this problem which require approaches distinct from the commonly studied quantum simulation of electronic structure: many eigenstates are often desired, states of interest are often far from the ground state (requiring methods for “zooming in” to some energy window), and transition amplitudes with respect to a non-unitary Hermitian operator must be calculated. We address these hurdles and consider problem instances of four vibrational Hamiltonians. Finally and most importantly, we give analytical and numerical results which strongly suggest that vibrational structure problems will achieve quantum advantage before electronic structure problems.

I. INTRODUCTION

To date, the vast majority of chemistry- and materials-related quantum algorithms research has focused on the electronic structure problem [1, 2]. Given a particular set of nuclear coordinates, the goal is to solve the fermionic (electronic) many-body problem to determine accurate energies. However, an accurate solution of the electronic structure problem is only one of the current challenges in computational chemistry and materials science. There are properties of interest for which the computational bottleneck is not the electronic structure problem, but rather an accurate quantum treatment of the molecular motion.

One such area is the calculation of vibrational spectra, as there is a large subset of molecules for which the electronic structure problem *is* classically tractable to subchemical accuracy while the quantum vibrational problem is not (see Figure 1). This is true for small molecules and clusters in several areas of spectroscopy: infrared spectra, Raman spectra, vibronic spectra, and ultrafast vibrational spectra, to name just a few [3–5]. Roughly

* nicolas.sawaya@intel.com

† daniel.tabor@tamu.edu

speaking, the electronic structure problem is harder the larger the molecule is and the more electron correlation that is present (due to *e.g.* transition metals elements). The vibrational structure problem, on the other hand, is hard for non-rigid or “fluxional” molecules as well as non-covalent complexes [6] such as aqueous clusters [7–10].

Even qualitatively correct vibrational spectra often require a rigorous quantum treatment because Fermi resonances, association bands, and other resonance effects can result from small coupling terms [3, 11–13]. The ability to calculate vibrational structure has many applications including fuel combustion [14], atmospheric science [15], astrochemistry [16, 17], and fundamental experiments in chemical physics [18, 19]. Other than vibrational spectra, problems that lie in the lower-left quadrant of Figure 1 include low-temperature thermodynamic calculations of some bulk solids [20] and quantum liquids [21].

Previous quantum computational studies in this area include analog quantum algorithms for quantum vibrations [22–25], digital quantum algorithms for finding vibrational states and/or overlaps [26–28], and approaches for which vibrational degrees of freedom are coupled to other systems [29–32]. The present work is distinct in that we address the calculation of transition intensities as well as the importance of high-lying excited states; and more importantly, we provide an illuminating comparative analysis with respect to the complexity of electronic structure.

Here, we present algorithms for calculating vibrational spectra on both near- and long-term hardware, focusing on vibrational infrared spectra. One of our contributions is identifying certain essential components that are required for this problem class, drawing attention to the algorithmic objectives that would not appear in most problems that involve Hamiltonian simulation. Many properties of this class of problems are significantly different from *e.g.* the electronic structure problem, which we introduce to the reader and demonstrate how to overcome. Finally, we compare resource counts to the electronic structure problem, postulating that a vibrational structure problem will achieve quantum advantage before an electronic structure problem instance.

From a Hamiltonian simulation perspective, it is worth noting three conceptual differences between the nature of the electronic structure problem and that of vibrational spectroscopy problems. First, when it is said that the “spectrum” is being calculated in molecular electronic structure, this normally refers to at most a handful of the lowest-lying electronic states. In contrast, in a vibrational problem one is almost always interested in many states,

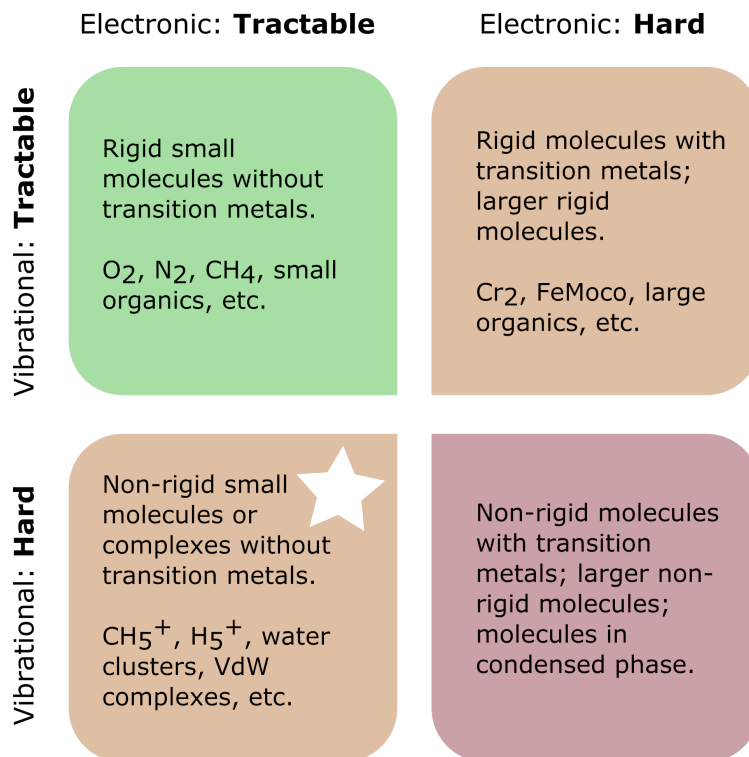


FIG. 1. We categorize molecular simulation in four quadrants, depending on whether the electronic structure and vibrational structure of the problem are tractable on a classical computer. Our focus is the lower-left quadrant—those molecules or complexes for which the potential energy surface can be calculated on a modern classical computer, while the quantum vibrational structure may require a quantum computer.

which may indeed be far from the ground state (excited states greater than 100 are often of interest).

The second conceptual difference is that one is often interested in calculating both vibrational energies and transition intensities, which necessitates calculating the transition amplitudes with respect to a non-unitary coordinate-dependent operator. Though such transition amplitudes (with respect to non-unitary Hermitian operators) are applicable to electronic structure in some important areas [33, 34], their inclusion is not the norm. Third, one is encoding bosons (vibrations) instead of fermions, a topic that has been previously explored [26, 35].

II. THEORY

Overview. In arbitrary internal coordinates \vec{s} (with corresponding momenta \vec{m}), the Hamiltonian for M vibrations in general form is written (with $\hbar = 1$)

$$H = \frac{1}{2} \sum g_{ij} m_i m_j + V(\vec{s}). \quad (1)$$

where g_{ij} is the coupling between momenta (vanishing for $i \neq j$ under normal or Cartesian coordinates) and $V(\vec{s})$ is the potential energy term. In the harmonic approximation, one may diagonalize the Hessian matrix at the equilibrium position, leading to a simplified approximate expression with uncoupled coordinates,

$$H_{\text{harm}} = \frac{1}{2} \sum_i^M \omega_i (q_i^2 + p_i^2), \quad (2)$$

where i denotes the vibrational mode, M is the total number of modes ($M = 3N - 5$ for linear molecules and $3M = N - 6$ for all others), q and p are respectively the bosonic position and momentum operators, and ω_i is the energy of mode i . It is trivial to find eigenvalue-eigenfunction pairs for equation (2) on a classical computer, since excited states in the Harmonic approximation are product states of separate modes.

Expression (2) can be systematically improved by including higher order terms,

$$H_{\text{anharm}} = \frac{1}{2} \sum_i^M \omega_i (q_i^2 + p_i^2) + \sum_{\{ijk\}} h_{ijk} q_i q_j q_k + \sum_{\{ijkl\}} h_{ijkl} q_i q_j q_k q_l + \dots, \quad (3)$$

where the index ordering is irrelevant and $h_{ijk\dots} = 0$ if all indices are distinct. Computational difficulties arise when these higher-order terms are included, due to both the deviation from harmonicity and the coupling between modes.

Even for a molecule of 5 to 10 atoms, the complete inclusion of anharmonic effects can be computationally prohibitive. Though various forms of perturbation theory and dimensionality reduction sometimes yield good results, one must often resort to exact diagonalization of the whole Hilbert space or similarly expensive methods [36–41]. We note that we are not constrained to use equation (3) but may choose any convenient coordinate system—it will often be the case that choosing a specialized coordinate system allows one to use a lower-order series expansion [42–44].

The dipole moment operator is also necessary for simulation light-matter interaction. It is denoted $\mu^{(\alpha)}$ where $\alpha \in \{x, y, z\}$ is a Cartesian direction. As $\mu^{(\alpha)}$ is coordinate-dependent,

it is associated with a dipole moment surface (DMS), which may be expanded in a power series,

$$\begin{aligned}\mu^{(\alpha)} &= \mu_0^{(\alpha)} + \sum_i^M \left. \frac{\partial \mu^{(\alpha)}}{q_i} \right|_{q_i=0} q_i + \frac{1}{2} \sum_{ij}^M \left. \frac{\partial^2 \mu^{(\alpha)}}{q_i q_j} \right|_{q_i, q_j=0} q_i q_j + \dots \\ &= \mu_0^{(\alpha)} + \sum_i^M m_i q_i + \sum_{ij}^M m_{ij} q_i q_j + \dots\end{aligned}\tag{4}$$

Both the Hamiltonian and the DMS operator may be mapped to a qubit-based Hamiltonian using the bosonic commutation relations, where a practical choice is to use the Pauli operator basis:

$$H_{\text{anharm}} \mapsto \sum_k^{N_P} a_k P_k = \sum_k a_k \bigotimes_g^{N_q} \sigma_{gk},\tag{5}$$

$$\mu^{(\alpha)} \mapsto \sum_k^{N_R^{(\alpha)}} b_{k\alpha} R_{k\alpha} = \sum_k b_{k\alpha} \bigotimes_g^{N_q} \sigma_{gk\alpha},\tag{6}$$

where g labels the qubit, $\sigma_g \in \{I, X, Y, Z\}$ is the identity or a Pauli operator, N_P ($N_R^{(\alpha)}$) is the number of Pauli strings in the encoded operator, and N_q is the number of qubits (see Appendix). Several encodings for performing this mapping have been discussed previously [26, 29, 35, 45], with evidence that the Gray code offers reasonable resource trade-offs [35].

In order to make our discussion concrete, we consider infrared spectroscopy, though similar mathematical methods would be used for other experiments such as Raman, microwave, or ultrafast multidimensional vibrational spectroscopy [3, 4]. The objective is to calculate

$$f(\omega) = \sum_{\alpha} \sum_j |\langle 0 | \mu^{(\alpha)} | j \rangle|^2 \mathcal{L}(\omega_j - \omega_0)\tag{7}$$

where $|0\rangle$ is the initial eigenstate (ground state when beginning from zero temperature) and $\mathcal{L}(\omega)$ is a line shape function, approximated as a delta function when one does not consider broadening effects. Though in this work we consider transitions from the ground state, the initial state of interest is often a Gibbs state (*i.e.* thermal state). Existing quantum algorithms for thermal state preparation [46–50] may be used in conjunction with the approaches summarized in this work. Note that expression (7) is mathematically similar

to what is used to calculate Franck-Condon factors [23, 27], where $\mu^{(\alpha)} = I$ and a different Hamiltonian is used.

An algorithm for the vibrational spectroscopy problem requires several elements: (a) mapping of bosons to qubits, (b) finding unitaries U_i to produce eigenstates, (c) determining state overlaps $|\langle\psi_i|\psi_j\rangle|^2$, (d) calculating transition amplitudes with respect to a non-unitary Hermitian operator, and (e) efficiently finding eigenstates far above the ground state. We first present the noisy intermediate-scale quantum (NISQ) approach for each problem requirement, before briefly summarizing a long-term approach that address all algorithmic requirements.

Near-term algorithms. Using near-term quantum hardware, ground and excited states may be found using previously published variational methods [48, 51–54]. For a given vibrational eigenstate $|\psi_j\rangle$, a variational method used with a classical optimizer will lead to a circuit unitary U_j as $U_j|0\rangle = |\psi_j\rangle$. Additionally, expression (7) requires a method for calculating state overlaps $|\langle\psi_i|\psi_j\rangle|^2$, for which quantum subroutines are summarized in the Appendix.

In order to calculate arbitrary transition amplitudes $|\langle\psi_i|\hat{A}|\psi_j\rangle|^2$ on near-term hardware, one needs an efficient method for calculating terms such as $\langle\psi_i|0\rangle$ or $\langle\psi_i|(\Pi_k\sigma_k)|0\rangle$ (where $(\Pi_k\sigma_k)$ is a Pauli string), in addition to their absolute values squared. This is a nontrivial task, since quantum computers naturally output overlaps squared. Though inner products may be calculated with so-called Hadamard tests that require a substantially increased circuit depth if only one- and two-qubit gates are allowed [55], a shorter-depth method was recently found [56] for calculating transition amplitudes of arbitrary operators. Tailoring the latter work to vibrational spectroscopy, the procedure is to use an additional set of unitaries,

$$V_{kl,\pm}^{(\alpha)} = \frac{1}{2}(I \pm R_{k\alpha})(I \pm R_{l\alpha}) = e^{\pm R_{k\alpha}\pi/4}e^{\pm R_{l\alpha}\pi/4} \quad (8)$$

for all $l, k < N_R^{(\alpha)}$. One then proceeds to reproduce $|\langle i|\mu^{(\alpha)}|j\rangle|^2$ from many measurements on the circuit set $U_i^\dagger V_{kl,\pm} U_j|0\rangle$ (see Appendix). Thus one increases the depth of two state preparation circuit by a small constant factor and collects measurement statistics from a quadratic (in N_p) number of circuits. This procedure is performed for every eigenenergy for which one wishes to calculate the transition amplitude.

Spectral window focusing. Not only are we often interested in many vibrational eigenstates—it is also often the case that one is concerned *only* with high-lying excited

states (for instance the 100th excited state and above). For example, part of a spectrum is often blocked by background noise; an astronomical telescope may be able to read only part of the infrared spectrum; or perhaps only a specific band is technologically relevant. Additionally, different regions of the spectrum contain different information. For example, in water clusters relevant to atmospheric chemistry, the OH stretches (3300 to 2500 cm^{-1}) report on local environments while the low-frequency region reports on collective motion [57]. Another example is terahertz spectroscopy, a newly accessible region of the electromagnetic spectrum that probes collective motion of molecules [58]. Therefore it may be a waste of computational effort to find eigenstates outside the energy window of interest.

The notable consequence is that most hereto proposed near-term algorithms for excited states are not viable. In their canonical forms, most existing near-term approaches [48, 51, 52, 59, 60] are appropriate only for low-lying states, though future modifications may render them appropriate.

We highlight one possible (previously proposed) near-term algorithmic solution for determining high-lying excited states. This is to use the folded spectrum method [53, 54], which easily allows one to select an energy neighborhood. The “folded” Hamiltonian is defined as

$$H_{fold} = (H - \zeta I)^2 \tag{9}$$

where ζ is an arbitrary constant. The lowest eigenstates of H_{fold} are those eigenstates of H which are closest in energy to ζ . This approach quadratically increases the number of Pauli terms in the effective Hamiltonian, allowing one to “zoom in” on an arbitrary portion of the spectrum. We do not rule out more efficient methods for high-lying excited states.

Utility of incomplete spectra. When using variational algorithms and NISQ hardware to determine portions of the spectra, it will often not be possible to know whether one has found all transitions in a given energy window. This is due to the nature of hybrid quantum-classical algorithms; it is usually not possible to guarantee that all eigenstates in a given energy region have been found. Hence it is important to note that even a spectrum with missing peaks is often useful. First, one may be interested in only a few specific spectral features in the region, in which case one may focus efforts converging to those specific transitions. Second, and perhaps more importantly, the goal is often to determine whether a candidate molecule matches an experimental result. If some spectral features in the theoretical spectrum of the candidate molecule are not present in the experimental

spectrum, then the candidate molecule can be removed from consideration.

Long-term hardware. A long-term fully error-corrected solution to these problems is to use quantum phase estimation (QPE) [61] to produce a probabilistic set of measurements. This approach has been discussed previously [27, 62, 63], first by Wecker and co-workers [62]. Using QPE on a superposition of eigenstates yields a superposition of eigenstate-eigenphase pairs

$$\sum c_i |\psi_i\rangle |0\rangle \xrightarrow{\text{QPE}} \sum c_i |\psi_i\rangle |\tilde{\phi}_i\rangle \quad (10)$$

where $\tilde{\phi}_i$ is the eigenphase $\exp(-iE_i)$, approximated to an arbitrary number of bits. This differs from the standard use of QPE, where the typical goal is to find a single eigenvalue. In calculating spectra, one instead begins in a mix of eigenstates representing the initial state of the molecule ($|0\rangle$) and collapses to each eigenenergy (eigenphase) with probability $f(\tilde{\omega})$. Because measuring the phase register yields a superposition of all states with approximate energy $\tilde{\phi}_i$, this method has the advantage of being able to calculate the full spectrum in polynomial time, despite a potentially exponential number of relevant eigenstates.

As discussed, vibrational (*e.g.* infrared) spectroscopy requires calculating the action of an arbitrary non-unitary operator $\mu^{(\alpha)}$ on a prepared state. When using QPE, the solution is to probabilistically implement the operator μ , as outlined in [63]. Using one ancilla qubit to apply the unitary

$$U_{\mu,\alpha,\gamma} = \begin{pmatrix} \cos \gamma \mu^{(\alpha)} & -\sin \gamma \mu^{(\alpha)} \\ \sin \gamma \mu^{(\alpha)} & \cos \gamma \mu^{(\alpha)} \end{pmatrix} \quad (11)$$

to an arbitrary state $|\psi\rangle$, will yield $\mathcal{N} \mu^{(\alpha)} |\psi\rangle$ with probability $P_{\text{success}} = \langle \psi | \sin(\gamma \mu^{(\alpha)}) | \psi \rangle$, where $\mathcal{N} = \|\mu^{(\alpha)} |\psi\rangle\|^{-1}$ is a normalization constant.

Finally, we posit that there are promising strategies for “spectral window focusing” in long-term hardware as well. For the QPE-based method, the goal would be to make the histogram measurements fall primarily within a particular energy window, as measurements outside the window are not of interest. Once the superposition of eigenstate-eigenphase pairs has been prepared (but before measurement), one may use amplitude amplification methods [64, 65] on the phase register to boost the probability of the desired eigenenergy window. The result is that fewer measurements would be required to produce the histogram

in the energy window of interest, at the cost of a slight increase in circuit depth. We leave a full description to future work.

III. COMPARISON TO ELECTRONIC STRUCTURE

The first physics simulation to achieve quantum advantage is likely to be a nearest-neighbor toy model such as an Ising model [66], because only $\mathcal{O}(N)$ two-body interactions are present. But it is important to consider what will be the first real-world non-toy simulation to show quantum advantage. Here we argue that the first such simulation of a molecule is more likely to be a vibrational problem instance than an electronic one.

The quantum resources required for the vibrational problem depend on the order of the expansion needed for sufficient precision in equation (3). We posit that early molecular targets for quantum computing ought to be those for which (a) classical computational approaches (*e.g.* perturbation theory) fail and (b) the highest relevant order is 4 or less (for scaling reasons given below). Both requirements are likely to hold for a substantial set of molecules [67, 68]. A third-order Hamiltonian has four types of terms: p_i^2 , q_i^2 , q_i^3 , $q_i^2 q_j$. A fourth-order Hamiltonian has 8 types with the inclusion of q_i^4 , $q_i^3 q_j$, $q_i^2 q_j^2$, and $q_i^2 q_j q_k$. Note that, depending on the choice of coordinate system, it is often possible to exclude three-body terms $q_i^2 q_j q_k$, while still obtaining sufficiently accurate results [42–44, 68]. The Appendix gives Pauli operator counts for each of these 8 term types, for $d = 4$ (2 qubits) and $d = 8$ (3 qubits).

The electronic structure Hamiltonian can be written

$$H_{\text{ES}} = \sum h_{ij} a_i^\dagger a_j + \sum h_{ijkl} a_i^\dagger a_j^\dagger a_k a_l, \quad (12)$$

where a_i^\dagger and a_i are fermionic creation/annihilation operators for the i th orbital and coefficients h_{ij} and h_{ijkl} are determined by calculating overlap integrals. 2- and 4-body terms are present, and in real molecules one has nearly all-to-all connectivity between the electronic orbitals. For simplicity we write equation (12) without spin constraints, though our results do take into account spin degrees of freedom (see Appendix).

Our argument will hinge on the notion that a Hamiltonian with more terms and with higher Pauli lengths is likely to require more resources to simulate, regardless of whether one is using near- or long-term hardware. A key insight is that 3rd- and 4th-order vibrational

Taylor terms in fact yield at most 2- and 3-body interactions, respectively, as every higher-order term necessarily includes q_i^2 in the product. This leads to either a $\mathcal{O}(M^2)$ or $\mathcal{O}(M^3)$ scaling in the number of terms for this subset of molecules, compared to $\mathcal{O}(N^4)$ for electronic structure of an arbitrary molecule, where N is the number of spin-orbitals. The argument is not complete though. One must still (a) determine whether the pre-factor to the vibrational problem is sufficiently small for lower qubit counts, and (b) investigate the distributions of lengths of the Pauli strings, both of which we study in the next section.

Notably, there has been extensive recent progress in reducing the asymptotic scaling of quantum algorithms for electronic structure [69–72]. However, due to these newer algorithms’ need for a larger basis set and/or an increase in the number of required qubits, these methods are not amenable to accurate molecular simulation for qubit counts below 100 [72]. Even if one assumes that error-corrected hardware is required for solving both the vibrational and electronic problems, it remains likely that the subset of vibrational problems with $\mathcal{O}(M^2)$ or $\mathcal{O}(M^3)$ Pauli terms will be solvable before any electronic structure instance, based on the analysis below.

One should assume that state-of-the-art methods will be used to reduce the number of qubits required to simulate any problem, leading to substantial reductions in the number of effective vibrational modes or electron orbitals. In vibrational problems, one may choose a coordinate system that is efficient in terms of having low truncation requirements and fewer appreciable coupling terms [5, 68]. For electronic structure, one carefully chooses the active space of orbitals [72–74]. Notably, it is more common to see sparser interactions in vibrational problems than in electronic structure problems, because it is often the case that some vibrational modes show negligible coupling to the other modes—this implies $\mathcal{O}(M^2)$ may often be an overestimate.

IV. RESULTS

Vibrational versus electronic. Figure 2 shows the number of Pauli terms in the Hamiltonian against the number of qubits. All vibrational data is for fourth-order Hamiltonians, where we use bosonic truncations $d = 4$ or 8 and have considered both the exclusion and inclusion of 3-body terms $q_i^2 q_j q_k$. Though the electronic structure problem scales as $\mathcal{O}(N^4)$ against the $\mathcal{O}(M^3)$ or $\mathcal{O}(M^2)$ vibrational scaling, the latter always have a larger leading

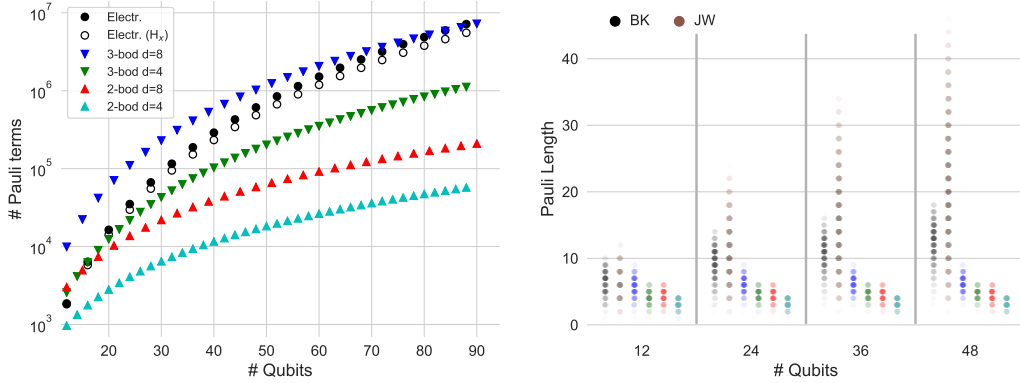


FIG. 2. *Left*: Number of Pauli strings in the qubit Hamiltonian versus the number of qubits, for the standard electronic structure problem and some classes of vibrational problem. Filled circles represent analytical results and unfilled circles represent numerical results from a collection of hydrogen atoms. Triangles represent analytical results for fourth-order vibrational Hamiltonians, where *e.g.* “3-bod $d=8$ ” signifies a truncation of 8 where three-body terms are included. *Right*: Probability distributions of Pauli lengths in six Hamiltonian classes. BK and JW respectively denote the Bravyi-Kitaev and Jordan-Wigner mappings for the electronic structure problem. All shown vibrational problems are fourth-order Hamiltonians.

coefficient (see Appendix). However, for the majority of cases considered here, these results show that the electronic structure Hamiltonians are more complex for qubit counts greater than ~ 20 .

For simplicity, we consider only cases in which all modes have equal d . In reality, each mode would require a different truncation, meaning that the number of Pauli strings would not exactly match one of the plots shown. For the electronic problem instances, the analytical results (filled circles) are comparable to the numerical results (open circles) obtained from 3D arrays of hydrogen atoms (see Appendix). Note that the number of Pauli terms is equal for the Jordan-Wigner (JW) [75] and Bravyi-Kitaev (BK) [76] encodings, though their length distributions are unequal.

The right panel of Figure 2 shows the distribution of Pauli lengths, another important indicator of a problem Hamiltonian’s complexity. For the subset of vibrational problem instances considered (fourth-order Hamiltonians with truncations of $d \leq 8$), vibrational problems are more local than electronic problems, even for low qubit counts when compared

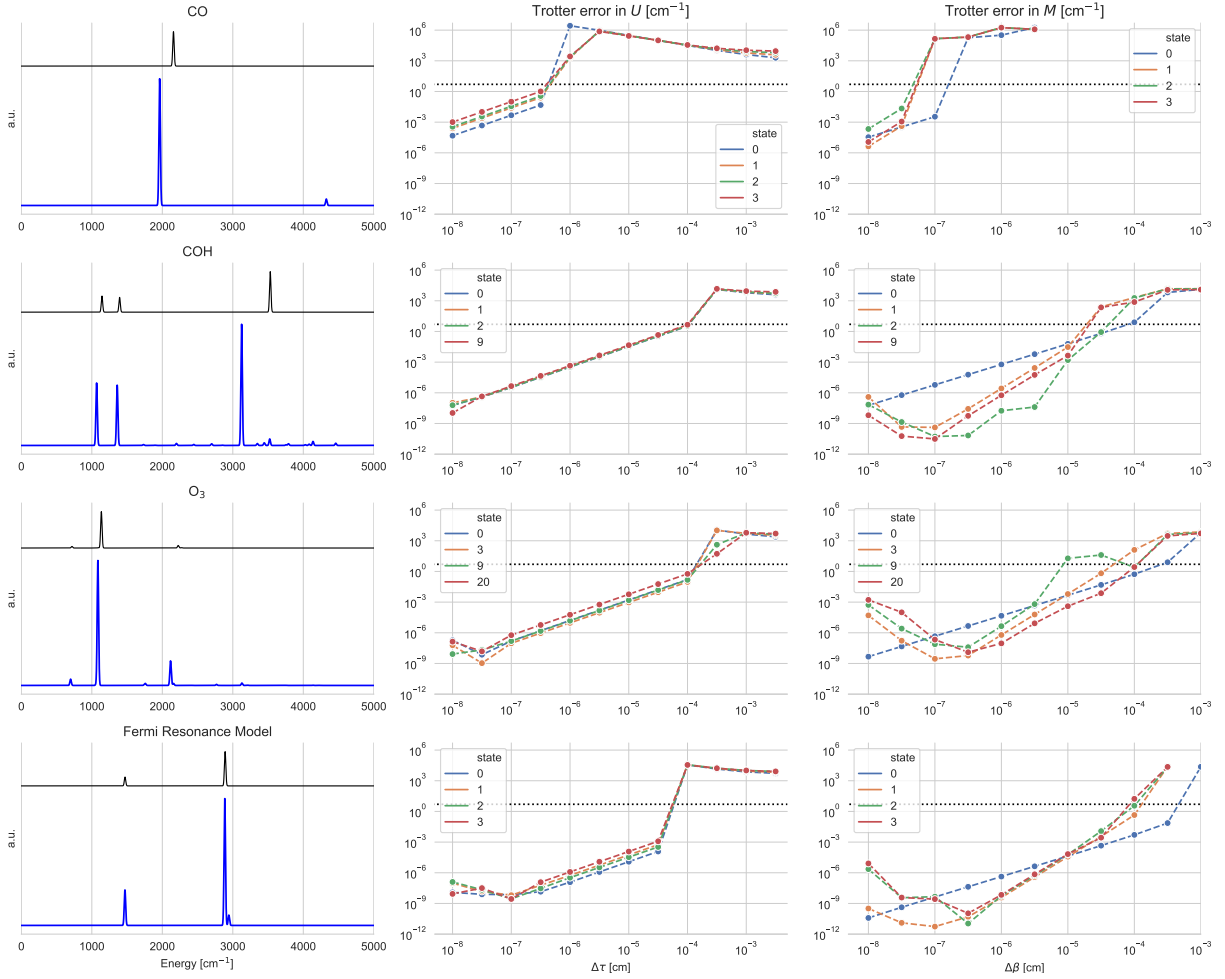


FIG. 3. Vibrational infrared spectra for our Fermi resonance model Hamiltonian, carbon monoxide (CO), the isoformyl radical (COH), and ozone (O_3). The first column shows the infrared spectra (blue) and its harmonic approximation (black) in arbitrary units, summing intensities in all Cartesian directions. Peaks were broadened with Gaussians of arbitrary standard deviation 10 cm^{-1} . The second column shows Trotterization error in the quantum time propagator, which is relevant to long-term algorithms. The third column shows Trotterization error in the imaginary time evolution operator, relevant to some NISQ approaches. Excited states in the third column are found using the folded Hamiltonian method. Horizontal dotted lines are at 5 cm^{-1} .

against the logarithmically scaling BK mapping.

These two results—that these vibrational Hamiltonians contain both fewer and shorter Pauli strings than their electronic counterparts—robustly support our postulate, that a vibrational problem instance is likely to achieve quantum advantage before an electronic

problem instance.

IR spectra. As a proof of principle, we performed numerical simulations on four vibrational Hamiltonians (see Appendix): carbon monoxide (CO), the isoformyl radical (COH), ozone (O_3), and a model Hamiltonian of Fermi resonance. Figure 3 shows the infrared spectra (blue). The harmonic approximations (black) are plotted, showing the importance of including higher-order anharmonic terms that are hard to simulate classically. Qualitative differences such as the extra peaks that appear (*e.g.* at 2940 cm^{-1} in the Fermi resonance Hamiltonian) tend to be difficult to obtain classically, often failing under perturbation theory [12, 68].

The second column shows the Trotterization error in some of the more intense eigenvalues against increasing $\Delta\tau$, the time step for approximating $e^{-i\Delta\tau\sum_k a_k P_k} \approx \prod_k e^{-i\Delta\tau a_k P_k}$. These are related to long-term algorithms, both in running QPE and in dynamical simulations. The third column approximates the imaginary time evolution (ITE) operator’s error by Trotterization with finite length $\Delta\beta$, the step size for approximating the ITE operator $e^{\Delta\beta\sum_k a_k P_k} \approx \prod_k e^{\Delta\beta a_k P_k}$. These are more relevant to NISQ algorithms, both for imaginary time evolution (ITE) [48] and variational ansatzes based on ITE [77]. Excited states in the third column are calculated using the folded spectrum method, in order to highlight the use of a method that disregards lower irrelevant excited states. Notably, all non-monotonic behavior in the ITE error plots arise from folded Hamiltonians—the cause of this behavior is intriguing but unclear. The resulting error trends give an indication of the step sizes needed for accurate simulation of small molecules, though more detailed study is needed.

V. OUTLOOK

Although molecular electronic structure is often the first candidate offered as a real-world application of near-term quantum computing, we have shown that it is more likely that molecular vibrational structure will be the first quantum computation application of a real substance. After considering previously unidentified requirements in designing quantum algorithms for vibrational spectra, we have presented approaches for solving this class of problems on both near-term and long-term quantum computers, addressing the components that make this distinct from the electronic structure problem: calculating transition amplitudes with respect to a non-unitary operator and calculating high-lying excited states.

Future research should focus on more detailed resource counts including estimates of circuit depth and gate complexity, as well as inclusion of rotational and other degrees of freedom. This work advances the applicability of quantum computation for atmospheric science, many biomolecular interactions, fuel combustion, gas-phase reactions, and astrochemistry, while suggesting that some focus for near-term quantum applications ought to shift to scientifically relevant vibrational problems.

ACKNOWLEDGMENTS

D.P.T. acknowledges support from Texas A&M University startup funding. Portions of this research were conducted with high performance research computing resources provided by Texas A&M University.

Appendix A: Mapping vibrations to qubits

The operator for a single d -level particle (included a truncated bosonic mode) may be expressed as

$$A = \sum_{l,l'=0}^{d-1} a_{l,l'} |l'\rangle\langle l|. \quad (\text{A1})$$

In order to use a qubit-based quantum computer, each level must first be mapped to a bit representation, then to a set of Pauli matrices. For example, a 4-level particle with an operator $B = |2\rangle\langle 3| + |3\rangle\langle 2|$ would map to

$$\begin{aligned} |2\rangle\langle 3| + |3\rangle\langle 2| &\xrightarrow{\text{Std. Binary}} |10\rangle\langle 11| + |11\rangle\langle 01| \\ &= |1\rangle\langle 1| \otimes |0\rangle\langle 1| + |1\rangle\langle 0| \otimes |1\rangle\langle 1| \\ &= \frac{1}{2} \left(\hat{X}_0 - \hat{Z}_1 \hat{X}_0 \right) \end{aligned} \quad (\text{A2})$$

where the least significant bit (qubit) is labelled 0. In the last step, the following identities are used:

$$|0\rangle\langle 1| = \frac{1}{2}(\hat{X} + i\hat{Y}) \equiv \hat{\sigma}^-, \quad (\text{A3})$$

$$|1\rangle\langle 0| = \frac{1}{2}(\hat{X} - i\hat{Y}) \equiv \hat{\sigma}^+, \quad (\text{A4})$$

$$|0\rangle\langle 0| = \frac{1}{2}(I + \hat{Z}), \quad (\text{A5})$$

$$|1\rangle\langle 1| = \frac{1}{2}(I - \hat{Z}). \quad (\text{A6})$$

In the case of vibrational (bosonic) degrees of freedom, we truncate at a level of d that preserves the accuracy we require [78, 79]. We use the Gray code for the numerics presented in this work; for a more thorough study of the choice and tradeoffs for different mappings, see reference [35].

Appendix B: QPE method for finding spectra

Assuming access to a fully error-corrected quantum computer, the appropriate long-term algorithm for calculating spectra is based on quantum phase estimation (QPE) [80]. QPE is normally discussed in the context of finding one particular eigenstate. The algorithm uses two quantum registers, which we call S (for the quantum state) and E (for the phase of the eigenenergy). Register S is loaded with an eigenstate, and register E is initialized to $|0\rangle^{\otimes N_E}$ where N_E is the number of qubits in that register. At the end of the QPE algorithm, measuring register E provides $\tilde{\phi}_i$, the N_E -bit approximation to the eigenphase $\phi_i = \exp(-i\theta E_i)$, where θ is arbitrarily chosen.

In the more standard use of QPE, one first attempts to prepare a state with as much overlap as possible with a particular eigenstate, *e.g.* the ground state. Then running QPE and measuring the energy registers leads the collapse of the desired state, with a probability equal to the overlap squared.

In this work, QPE is instead used in a way that allows one to calculate a full response spectrum [27, 62, 63], *i.e.* determining the non-negligible values $|\langle \eta_0 | \hat{A} | \psi_i \rangle|^2$, where $\hat{A} | \eta_0 \rangle$ is not necessarily an eigenstate of the Hamiltonian but the $\{ | \psi_i \rangle \}$ are eigenstates. First consider the case of $\hat{A} = \hat{I}$. One runs the same QPE algorithm, but sets the initial state to a state $|\eta_0\rangle$, which is in general not an eigenstate, such that $|\eta_0\rangle = \sum_i c_i |\psi_i\rangle$. After running QPE, one is left with a superposition of eigenstate-eigenphase pairs, as shown in the expression (reproduced from the main text)

$$\sum c_i |\psi_i\rangle |0\rangle \xrightarrow{\text{QPE}} \sum c_i |\psi_i\rangle |\tilde{\phi}_i\rangle. \quad (\text{B1})$$

In contrast to the standard use of QPE, in this case we are interested in more than just one eigenstate. The algorithm proceeds as follows. One performs many repetitions of the circuit, measuring register E after each run, yielding a phase $\tilde{\phi}_i$. From many measurements one then composes a histogram where each bin is an N_E -bit value $\tilde{\phi}_i$. This histogram is the desired response spectrum with resolution determined by N_E , and the process terminates once the histogram has converged.

Importantly, one advantage of this method is that it effectively combines many eigenstates into a single measurement. For a particular N_E , there is a subset of eigenstates $\mathcal{D}_j = \{\psi_{j1}, \psi_{j2} \dots\}$ all of which yield $\tilde{\phi}_j$. Hence if the measurement yields $\tilde{\phi}_j$, this means register S has collapsed to the superposition $\mathcal{N} \sum_{k \in \mathcal{D}_j} c_k |\psi_k\rangle$, where \mathcal{N} is a normalization constant. The beneficial result is that the probabilities of many eigenenergies tend to be combined, and the number of required measurements is dependent on N_E but independent of the size of the problem Hamiltonian's Hilbert space.

Roggero *et al.* [63] solved the problem of linear response with respect to a non-unitary operator. After adding one ancilla qubit, one may implement the operator $U_{\mu, \alpha, \gamma}$, defined in the main text. This unitary probabilistically produces the desired state $|\Phi_0^{(\alpha)}\rangle \equiv \hat{\mu}^{(\alpha)}|\eta_0\rangle / \|\hat{\mu}^{(\alpha)}|\eta_0\rangle\|$. If the ancilla is measured to be $|0\rangle$ ($|1\rangle$) then the state preparation has succeeded (failed). The remainder of the algorithm then proceeds as in the $\hat{A} = \hat{I}$ case, with $|\eta_0\rangle$ replaced by $|\Phi_0^{(\alpha)}\rangle$.

Appendix C: Counting for fermionic operators

Here we summarize how the Pauli string counts were determined for molecular Hamiltonians. The electronic structure Hamiltonian takes the form shown in the main text, though with spin degrees of freedom it is written

$$H_{ES} = \sum_{p\sigma q\tau} h_{p\sigma, q\tau} a_{p\sigma}^\dagger a_{q\tau} + \sum_{pqrs\sigma\tau\mu\nu} h_{p\sigma, r\mu, s\nu, q\tau} a_{p\sigma}^\dagger a_{r\mu}^\dagger a_{s\nu} a_{q\tau} \quad (\text{C1})$$

where Latin letters label spatial orbitals and Greek letters label spin DOFs.

We assume that a real (as opposed to complex) basis is used. Fermionic commutation rules and spin orthogonality lead to the following symmetries [81]. First,

$$h_{PQRS} = h_{RSPQ} \quad (\text{C2})$$

and

$$h_{PQRS} = h_{QPRS} = h_{PQSR} = h_{QPSR}, \quad (\text{C3})$$

which leads to an eight-fold symmetry. Including orthogonality of spin degrees of freedom leads to

$$h_{p\sigma, q\tau, r\mu, s\nu} = h_{pqrs} \delta_{\sigma\tau} \delta_{\mu\nu}. \quad (\text{C4})$$

Finally, the following terms vanish:

$$\{a_i^\dagger a_i^\dagger a_j a_j, a_j^\dagger a_j^\dagger a_i a_i\} \rightarrow 0, \quad (\text{C5})$$

$$a_i^\dagger a_i^\dagger a_i a_i \rightarrow 0, \quad (\text{C6})$$

$$a_i^\dagger a_i^\dagger a_j a_k \rightarrow 0. \quad (\text{C7})$$

For each category of fermionic Hamiltonian term, we now consider the number of Pauli strings resulting from the Jordan-Wigner mapping, though the Pauli string count (but not the locality) is the same for the Bravyi-Kitaev mapping. The Jordan-Wigner encoding maps fermionic degrees of freedom to qubits such that fermionic commutation relations are retained. The mapping is defined as

$$\begin{aligned} a_p^\dagger &\mapsto \left(\prod_{m<p} Z_m \right) \sigma_p^+ \\ a_p^\dagger &\mapsto \left(\prod_{m<p} Z_m \right) \sigma_p^- \end{aligned} \quad (\text{C8})$$

where $\sigma^\pm \equiv (X \mp iY)/2$.

In our counting procedure, we avoid double-counting Pauli terms. For instance, terms like Z_i appear in both one- and two-electron operators, but they are counted only once.

The one-electron terms lead to

$$a_i^\dagger a_i \rightarrow Z + I = \frac{1}{2}(I - Z_i) \quad (\text{C9})$$

and

$$a_i^\dagger a_j + a_j^\dagger a_i \rightarrow \frac{1}{2}(X_i Z^{\otimes j-i-1} X_j + Y_i Z^{\otimes j-i-2} Y_j). \quad (\text{C10})$$

Non-vanishing two-body two-electron terms lead to

$$a_i^\dagger a_j^\dagger a_j a_i + a_j^\dagger a_i^\dagger a_i a_j \rightarrow \{I, Z_i, Z_j, Z_i Z_j\} \quad (\text{C11})$$

Based on the above symmetries, non-vanishing three-body terms lead to

$$\begin{aligned} & \{a_i^\dagger a_j^\dagger a_k a_i, \dots\}_{(4)} \cup \{a_i^\dagger a_j^\dagger a_i a_k, \dots\}_{(4)} \rightarrow 4 \text{ Pauli strings} \\ & \text{Example: } \{a_0^\dagger a_1^\dagger a_2 a_0, \dots\}_{(4)} \cup \{a_0^\dagger a_1^\dagger a_0 a_2, \dots\}_{(4)} \\ & \rightarrow \{Z_0 X_2 X_3, Z_0 Y_2 Y_3, X_2 X_3, Y_2 Y_3\} \end{aligned} \quad (\text{C12})$$

where each set of four operators leads to the same set of Pauli strings. Subscripts denote the number of Pauli strings in the bracketed set.

Finally, consider four-body terms with 8-fold symmetry. One such set of terms leads to four Pauli strings:

$$\begin{aligned} & \{a_i^\dagger a_k^\dagger a_l a_j, \dots\}_{(4)} \rightarrow 4 \text{ Pauli strings} \\ & \text{Example: } \{a_1^\dagger a_3^\dagger a_5 a_7, \dots\}_{(4)} \rightarrow \{X_1 Z_2 X_3 Y_5 Z_6 Y_7, \\ & \quad X_1 Z_2 Y_3 Y_5 Z_6 X_7, \\ & \quad Y_1 Z_2 X_3 X_5 Z_6 Y_7, \\ & \quad Y_1 Z_2 Y_3 X_5 Z_6 X_7\} \end{aligned} \quad (\text{C13})$$

To numerically validate our manual counting procedure, we used OpenFermion [82] and Psi4 [83] to calculate the number of Pauli strings required for the electronic structure problem of a collection of hydrogen atoms. Hydrogen atoms were placed on a cubic lattice with spacing 0.6 Å, with a random perturbation in each direction drawn from a Gaussian of standard deviation 0.05 Å. We used the minimal STO-3G basis, resulting in a number of qubits equal to 4 times the number of hydrogen atoms. The canonical orbitals used were determined from the Hartree-Fock calculation of Psi4. All Pauli string counts were within 10% to 30% of our manual analytical counts, a difference that we attribute primarily to the software truncating terms smaller than 10^{-6} .

Appendix D: Counting for bosonic operators

A third-order vibrational Hamiltonian in normal coordinates has four types of terms: p_i^2 , q_i^2 , q_i^3 , $q_i^2 q_j$. A fourth-order Hamiltonian has eight types, with the inclusion of q_i^4 , $q_i^3 q_j$, $q_i^2 q_j^2$, and $q_i^2 q_j q_k$.

All of our mappings use the Gray code [35]. Here we provide the Pauli mappings or Pauli counts for the different types of many-body terms, for both $d=4$ and 8. These are used for counting the number of terms in each type of Hamiltonian.

— Harmonic: —

$$\begin{aligned} p_0^2 + q_0^2 &\xrightarrow{d=4} 4I - 1Z_0Z_1 - 2Z_1 \\ &\xrightarrow{d=8} 8I - 1Z_0Z_1Z_2 \end{aligned} \quad (\text{D1})$$

— 3rd-order: —

$$\begin{aligned} q_i^3 &\xrightarrow{d=4} \{X_0, X_0Z_1, Z_0X_1, X_1\} \\ &\xrightarrow{d=8} (16 \text{ Pauli strings}) \end{aligned} \quad (\text{D2})$$

$$\begin{aligned} q_i^2 q_j &\xrightarrow{d=4} (20 \text{ Pauli strings}) \\ &\xrightarrow{d=8} (144 \text{ Pauli strings}) \end{aligned} \quad (\text{D3})$$

— 4th-order: —

$$\begin{aligned} q_i^4 &\xrightarrow{d=4} (\text{I} \& \text{ 5 Pauli strings}) \\ &\xrightarrow{d=8} (\text{I} \& \text{ 18 Pauli strings}) \end{aligned} \quad (\text{D4})$$

$$\begin{aligned} q_i^3 q_j &\xrightarrow{d=4} (16 \text{ Pauli strings}) \\ &\xrightarrow{d=8} (192 \text{ Pauli strings}) \end{aligned} \quad (\text{D5})$$

$$\begin{aligned} q_i^2 q_j^2 &\xrightarrow{d=4} (\text{I} \& \text{ 24 Pauli strings}) \\ &\xrightarrow{d=8} (144 \text{ Pauli strings}) \end{aligned} \quad (\text{D6})$$

$$\begin{aligned} q_i^2 q_j q_k &\xrightarrow{d=4} (80 \text{ Pauli strings}) \\ &\xrightarrow{d=8} (1728 \text{ Pauli strings}) \end{aligned} \quad (\text{D7})$$

In order to numerically validate our counting procedure, we prepared vibrational Hamiltonians with randomized non-zero couplings for all possible terms up to fourth order. We omitted some results from the main text in order to avoid over-crowding the figure. The analytical and numerical results for all Hamiltonians are shown in Figure 4.

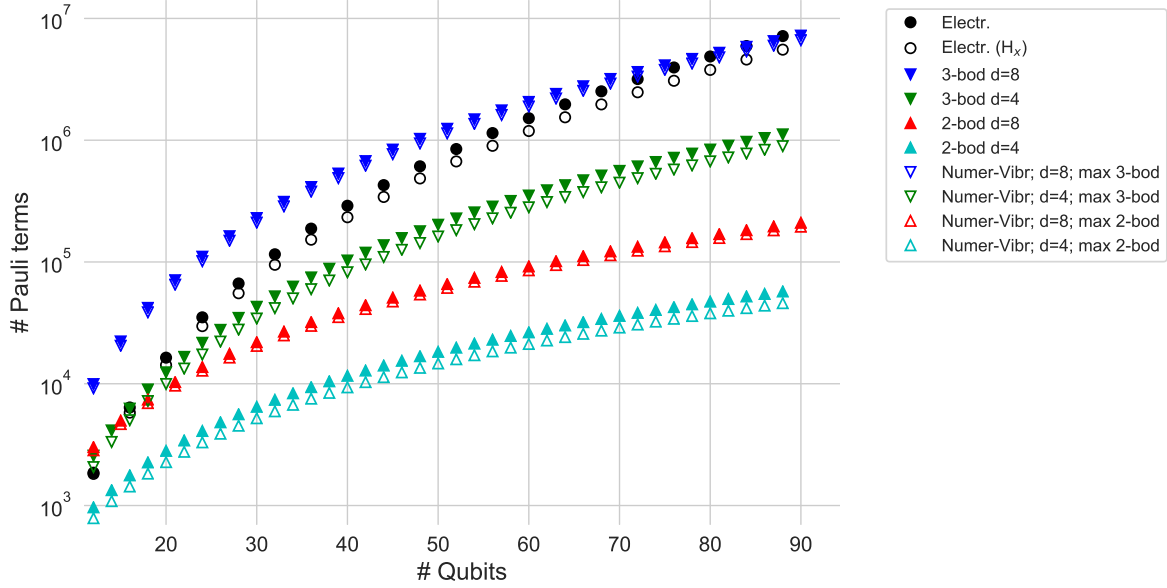


FIG. 4. Pauli string counts, including both analytical and numerical (random vibrational Hamiltonian) results.

Appendix E: Potential energy and dipole surfaces

The potential energy surface and dipole derivatives for CO and COH were calculated at the CCSD(T)/ANO1 level with the CFOUR package, version 2.1 [84]. We used the package’s documented scripts for calculating anharmonic frequencies by finite differences in parallel to obtain the quadratic, cubic, and quartic (including three-body) force constants.

All energy units are cm^{-1} . The resulting fourth-order Hamiltonian for carbon monoxide is

$$H_{CO} = 2157.96 \frac{q^2 + p^2}{2} - 736.66 q^3 + 210.97 q^4. \quad (\text{E1})$$

The fourth-order Hamiltonian for the isoformyl radical is

$$\begin{aligned}
H_{COH} = & 1143.24 \frac{q_1^2 + p_1^2}{2} \\
& + 1393.46 \frac{q_2^2 + p_2^2}{2} \\
& + 3530.65 \frac{q_3^2 + p_3^2}{2} \\
& + -16.83 q_1 q_1 q_1 + 51.76 q_1 q_1 q_2 \\
& + 40.02 q_1 q_2 q_2 + 87.05 q_2 q_2 q_2 \\
& + 413.74 q_1 q_1 q_3 - 116.13 q_1 q_2 q_3 \\
& - 35.26 q_2 q_2 q_3 - 92.65 q_1 q_3 q_3 \\
& - 119.29 q_2 q_3 q_3 - 489.34 q_3 q_3 q_3 \\
& + 22.83 q_1 q_1 q_1 q_1 - 10.84 q_1 q_1 q_1 q_2 \\
& - 10.48 q_1 q_1 q_1 q_3 - 0.49 q_1 q_1 q_2 q_2 \\
& - 40.20 q_1 q_1 q_2 q_3 - 252.07 q_1 q_1 q_3 q_3 \\
& + 7.00 q_1 q_2 q_2 q_2 - 3.37 q_1 q_2 q_2 q_3 \\
& + 6.96 q_2 q_2 q_2 q_2 - 6.15 q_2 q_2 q_2 q_3 \\
& - 17.44 q_2 q_2 q_3 q_3 + 26.32 q_1 q_2 q_3 q_3 \\
& - 3.13 q_1 q_3 q_3 q_3 - 4.33 q_2 q_3 q_3 q_3 \\
& + 66.64 q_3 q_3 q_3 q_3,
\end{aligned} \tag{E2}$$

where q_1 is the bending mode, q_2 is the CO stretch, and q_3 is the OH stretch.

The first-order transition dipoles were found to be

$$\begin{aligned}
\mu^{(x)} & \sim -0.33854 q_1 - 0.268687 q_2 - 0.011334 q_3 \\
\mu^{(y)} & \sim -0.057874 q_1 - 0.023912 q_2 + 0.175823 q_3
\end{aligned} \tag{E3}$$

where the equilibrium dipole is irrelevant because it cancels out due to orthogonality when one begins from the ground state. Units are in Debye, though we considered only relative intensities in our calculations.

For ozone (isotope $^{16}\text{O}_3$) we used previously published PES [85] and DMSs [86]. The surfaces for our Fermi resonance Hamiltonian is described in the next section.

Appendix F: Model Hamiltonian for Fermi Resonances

Our model Hamiltonian for Fermi resonances has two vibrational modes, taking the form

$$\hat{H}_{FR} = \omega_0 \left(a_0^\dagger a_0 + \frac{1}{2} \right) + \omega_1 \left(a_1^\dagger a_1 + \frac{1}{2} \right) + h_{001} q_0^2 q_1 \quad (\text{F1})$$

We choose frequencies and couplings that are typical for the bending and stretching modes of two CH stretches within a methyl (CH₃) functional group, a well-known example of Fermi resonance. We set $\omega_0 = 1470 \text{ cm}^{-1}$ (bend), $\omega_1 = 2890 \text{ cm}^{-1}$ (stretch), and $h_{001} = 30 \text{ cm}^{-1}$ [12]. A necessary condition for Fermi resonance is that $\omega_1 \approx 2\omega_0$, which is met here as $\omega_1/\omega_0 \approx 1.966$. In our model calculations, for the first-order Taylor terms of dipole moment surface μ we set $m_0 = m_1$.

Appendix G: NISQ method for transition amplitudes

Before summarizing the method for calculating arbitrary transition amplitudes, we give two known methods for calculating $|\langle \eta_i | \eta_j \rangle|^2$, an important primitive. In the first method, one implements $U_i^\dagger U_j$. Thereafter, the fraction of measurements that equal the all-zero vector $|0\rangle^{\otimes N_q}$ is equal to the overlap squared [87]. This method does not require additional qubits though it approximately doubles the circuit depth. The second method is to use a SWAP test [88] or destructive SWAP test [89], which doubles the number of qubits but increased the depth only by a small constant factor.

The near-term algorithm for transition amplitudes $|\langle i | \mu^{(\alpha)} | j \rangle|^2$ is based on work by Ibe and coworkers [56]. Applying their methodology to our operators, the result is

$$\begin{aligned} |\langle i | \mu^{(\alpha)} | j \rangle|^2 = & \sum_k b_{k\alpha}^2 |\langle i | R_{k\alpha} | j \rangle|^2 \\ & + \sum_{k < l} b_{k\alpha} b_{l\alpha} \left[2 |\langle i | V_{kl,+}^{(\alpha)} | j \rangle|^2 + 2 |\langle i | V_{ij,-}^{(\alpha)} | j \rangle|^2 \right. \\ & \left. - |\langle i | R_{k\alpha} | j \rangle|^2 - |\langle i | R_{l\alpha} | j \rangle|^2 - |\langle i | R_{l\alpha} R_{k\alpha} | j \rangle|^2 \right]. \end{aligned} \quad (\text{G1})$$

Terms $|\langle i | V_{kl,\pm}^{(\alpha)} | j \rangle|^2$ are determined by preparing the state $U_i^\dagger V_{kl,\pm}^{(\alpha)} U_j |0\rangle$. Terms such as $|\langle i | R_{k\alpha} | j \rangle|^2$ are determined by preparing state

$$U_i^\dagger \exp(i\frac{\pi}{2}R_{k\alpha})U_j|0\rangle$$

and counting zero strings. Expressions $\exp(\pm i\theta R_{k\alpha})$ can be implemented in short depth using well known primitives [90]. The number of required circuits scales quadratically with the number of Pauli strings $N_R^{(\alpha)}$ in $\mu^{(\alpha)}$.

The advantage of Ibe et al.’s approach is that Hadamard tests [55] are not needed. Hadamard tests would require controlled- U_i unitaries. Assuming the quantum hardware uses one- and two-qubit gates, this would often require each three-qubit gate to be decomposed into many one- and two-qubit gates [90], considerably increasing the circuit depth.

Appendix H: Analysis of Trotter error

We studied Trotter error for both the approximate unitary used in QPE and the approximate imaginary time evolution operator appropriate for nearer-term algorithms. For the former case, we constructed the unitary matrix

$$\tilde{U}(\Delta\tau) = \prod_k^{N_P} e^{-i\Delta\tau a_k P_k}. \quad (\text{H1})$$

where $\Delta\tau$ is the time step. This is a first-order Trotter approximation to the quantum propagator $U(\Delta\tau) \equiv \exp(-i\Delta\tau H)$. We then diagonalized $\tilde{U}(\Delta\tau)$ and compared the ordered eigenvalues to the exact result.

In our simulation of imaginary time evolution, we instead constructed the operator

$$\tilde{M}(\Delta\beta) = \prod_k^{N_P} e^{-\Delta\beta a_k P_k} \quad (\text{H2})$$

where $\Delta\beta$ is an imaginary time step. For all but the ground state, equation H2 used the Pauli representation of the folded Hamiltonian, not the original Hamiltonian. Folded Hamiltonians were used in order to highlight the use of a method that allows one to skip irrelevant eigenstates, effectively implementing spectral window focusing. Calculations were implemented using Scipy [91].

Errors in U are mostly independent of the eigenstates, while errors in M are distributed over many orders of magnitude even for fixed $\Delta\beta$. This may be partly because each folded Hamiltonian is in fact a different Hamiltonian. CO requires the smallest (*i.e.* worst)

timestep, which we hypothesize might be due to the lack of favorable error cancellation, as cancellation may be more prominent in Hamiltonians with more terms. There was no clear trend with respect to the (Froebenius) norms of the Hamiltonians, though in the worse case (carbon monoxide) the error becomes unacceptably large approximately when $\Delta\tau$ and $\Delta\beta$ have order of magnitude comparable to the inverse norm of the Hamiltonian ($1/\|H\|$). Further study is needed to determine broadly applicable relationships between vibrational problem instances and Trotter error.

-
- [1] Y. Cao, J. Romero, J. P. Olson, M. Degroote, P. D. Johnson, M. Kieferová, I. D. Kivlichan, T. Menke, B. Peropadre, N. P. D. Sawaya, S. Sim, L. Veis, and A. Aspuru-Guzik, Quantum chemistry in the age of quantum computing, *Chemical Reviews* **119**, 10856 (2019).
 - [2] S. McArdle, S. Endo, A. Aspuru-Guzik, S. C. Benjamin, and X. Yuan, Quantum computational chemistry, *Rev. Mod. Phys.* **92**, 015003 (2020).
 - [3] P. F. Bernath, *Spectra of Atoms and Molecules (Second Edition)* (Oxford University Press, New York, 2005).
 - [4] S. Mukamel, *Principles of Nonlinear Optical Spectroscopy* (Oxford University Press, 1999).
 - [5] E. B. Wilson, J. C. Decius, and P. C. Cross, *Molecular Vibrations: The Theory of Infrared and Raman Vibrational Spectra* (Dover Publications, Mineola, NY, USA, 1980).
 - [6] P. Jankowski, A. R. W. McKellar, and K. Szalewicz, Theory untangles the high-resolution infrared spectrum of the ortho-H₂-CO van der waals complex, *Science* **336**, 1147 (2012).
 - [7] S. E. Brown, A. W. Gtz, X. Cheng, R. P. Steele, V. A. Mandelshtam, and F. Paesani, Monitoring water clusters melt through vibrational spectroscopy, *Journal of the American Chemical Society* **139**, 7082 (2017).
 - [8] M. Riera, S. E. Brown, and F. Paesani, Isomeric equilibria, nuclear quantum effects, and vibrational spectra of M+(H₂O)_{n=13} clusters, with M = Li, Na, K, Rb, and Cs, through many-body representations, *The Journal of Physical Chemistry A* **122**, 5811 (2018).
 - [9] P. Bajaj, J. O. Richardson, and F. Paesani, Ion-mediated hydrogen-bond rearrangement through tunnelling in the iodide–dihydrate complex, *Nature Chemistry* **11**, 367 (2019).
 - [10] N. Yang, C. H. Duong, P. J. Kelleher, A. B. McCoy, and M. A. Johnson, Deconstructing water’s diffuse OH stretching vibrational spectrum with cold clusters, *Science* **364**, 275 (2019).

- [11] J. Vázquez and J. F. Stanton, Treatment of Fermi resonance effects on transition moments in vibrational perturbation theory, *Molecular Physics* **105**, 101 (2007).
- [12] E. L. Sibert, D. P. Tabor, N. M. Kidwell, J. C. Dean, and T. S. Zwier, Fermi resonance effects in the vibrational spectroscopy of methyl and methoxy groups, *The Journal of Physical Chemistry A* **118**, 11272 (2014).
- [13] A. B. McCoy, T. L. Guasco, C. M. Leavitt, S. G. Olesen, and M. A. Johnson, Vibrational manifestations of strong non-condon effects in the $\text{H}_3\text{O}+\text{X}_3$ ($\text{X} = \text{Ar}, \text{N}_2, \text{CH}_4, \text{H}_2\text{O}$) complexes: A possible explanation for the intensity in the association band in the vibrational spectrum of water, *Phys. Chem. Chem. Phys.* **14**, 7205 (2012).
- [14] L. B. Harding, Y. Georgievskii, and S. J. Klippenstein, Accurate anharmonic zero-point energies for some combustion-related species from diffusion Monte Carlo, *The Journal of Physical Chemistry A* **121**, 4334 (2017).
- [15] G.-L. Hou, W. Lin, S. H. M. Deng, J. Zhang, W.-J. Zheng, F. Paesani, and X.-B. Wang, Negative ion photoelectron spectroscopy reveals thermodynamic advantage of organic acids in facilitating formation of bisulfate ion clusters: Atmospheric implications, *The Journal of Physical Chemistry Letters* **4**, 779 (2013).
- [16] V. Barone, M. Biczysko, and C. Puzzarini, Quantum chemistry meets spectroscopy for astrochemistry: Increasing complexity toward prebiotic molecules, *Accounts of Chemical Research* **48**, 1413 (2015).
- [17] B. A. McGuire, A. M. Burkhardt, S. Kalenskii, C. N. Shingledecker, A. J. Remijan, E. Herbst, and M. C. McCarthy, Detection of the aromatic molecule benzonitrile ($c\text{-C}_6\text{H}_5\text{CN}$) in the interstellar medium, *Science* **359**, 202 (2018).
- [18] S. Ospelkaus, K.-K. Ni, G. Quéméner, B. Neyenhuis, D. Wang, M. H. G. de Miranda, J. L. Bohn, J. Ye, and D. S. Jin, Controlling the hyperfine state of rovibronic ground-state polar molecules, *Phys. Rev. Lett.* **104**, 030402 (2010).
- [19] R. F. Ribeiro, L. A. Martinez-Martinez, M. Du, J. Campos-Gonzalez-Angulo, and J. Yuen-Zhou, Polariton chemistry: controlling molecular dynamics with optical cavities, *Chem. Sci.* **9**, 6325 (2018).
- [20] V. Kapil, E. Engel, M. Rossi, and M. Ceriotti, Assessment of approximate methods for anharmonic free energies, *Journal of Chemical Theory and Computation* **15**, 5845 (2019).
- [21] A. J. Leggett, *Quantum Liquids: Bose Condensation and Cooper Pairing in Condensed-Matter*

- Systems*, 1st ed. (Oxford University Press, 2006).
- [22] S. Joshi, A. Shukla, H. Katiyar, A. Hazra, and T. S. Mahesh, Estimating Franck-Condon factors using an NMR quantum processor, *Phys. Rev. A* **90**, 022303 (2014).
- [23] J. Huh, G. G. Guerreschi, B. Peropadre, J. R. McClean, and A. Aspuru-Guzik, Boson sampling for molecular vibronic spectra, *Nature Photonics* **9**, 615 (2015), 1412.8427.
- [24] A. Teplukhin, B. K. Kendrick, and D. Babikov, Calculation of molecular vibrational spectra on a quantum annealer, *Journal of Chemical Theory and Computation* **15**, 4555 (2019).
- [25] C. Sparrow, E. Martín-López, N. Maraviglia, A. Neville, C. Harrold, J. Carolan, Y. N. Joglekar, T. Hashimoto, N. Matsuda, J. L. O’Brien, D. P. Tew, and A. Laing, Simulating the vibrational quantum dynamics of molecules using photonics, *Nature* **557**, 660 (2018).
- [26] S. McArdle, A. Mayorov, X. Shan, S. Benjamin, and X. Yuan, Digital quantum simulation of molecular vibrations, *Chemical Science* **10**, 5725 (2019).
- [27] N. P. D. Sawaya and J. Huh, Quantum algorithm for calculating molecular vibronic spectra, *The Journal of Physical Chemistry Letters* **10**, 3586 (2019).
- [28] P. J. Ollitrault, A. Baiardi, M. Reiher, and I. Tavernelli, Hardware efficient quantum algorithms for vibrational structure calculations, *Chemical Science* **11**, 6842 (2020).
- [29] L. Veis, J. Višňák, H. Nishizawa, H. Nakai, and J. Pittner, Quantum chemistry beyond Born-Oppenheimer approximation on a quantum computer: A simulated phase estimation study, *Int. J. Quantum Chem.* **116**, 1328 (2016).
- [30] A. Macridin, P. Spentzouris, J. Amundson, and R. Harnik, Electron-phonon systems on a universal quantum computer, *Phys. Rev. Lett.* **121**, 110504 (2018).
- [31] A. B. Magann, M. D. Grace, H. A. Rabitz, and M. Sarovar, Digital quantum simulation of molecular dynamics and control (2020), arXiv:2002.12497.
- [32] P. J. Ollitrault, G. Mazzola, and I. Tavernelli, Non-adiabatic molecular quantum dynamics with quantum computers (2020), arXiv:2006.09405.
- [33] T. Kosugi and Y.-i. Matsushita, Linear-response functions of molecules on a quantum computer: Charge and spin responses and optical absorption, *Phys. Rev. Research* **2**, 033043 (2020).
- [34] X. Cai, W.-H. Fang, H. Fan, and Z. Li, Quantum computation of molecular response properties (2020), arXiv:2001.03406.
- [35] N. P. D. Sawaya, T. Menke, T. H. Kyaw, S. Johri, A. Aspuru-Guzik, and G. G. Guerreschi,

- Resource-efficient digital quantum simulation of d-level systems for photonic, vibrational, and spin-s Hamiltonian, *npj Quantum Information* **6**, 49 (2020).
- [36] J. C. Light and Z. Bačić, Adiabatic approximation and nonadiabatic corrections in the discrete variable representation: Highly excited vibrational states of triatomic molecules, *The Journal of Chemical Physics* **87**, 4008 (1987).
- [37] E. L. Sibert, Theoretical studies of vibrationally excited polyatomic molecules using canonical Van Vleck perturbation theory, *The Journal of Chemical Physics* **88**, 4378 (1988).
- [38] X.-G. Wang and T. Carrington, Vibrational energy levels of CH₅⁺, *The Journal of Chemical Physics* **129**, 234102 (2008).
- [39] J. M. Bowman, T. Carrington, and H.-D. Meyer, Variational quantum approaches for computing vibrational energies of polyatomic molecules, *Molecular Physics* **106**, 2145 (2008).
- [40] A. van der Avoird and D. J. Nesbitt, Rovibrational states of the H₂O–H₂ complex: An ab initio calculation, *The Journal of Chemical Physics* **134**, 044314 (2011).
- [41] Z. Lin and A. B. McCoy, Probing the Relationship Between Large-Amplitude Motions in H₅⁺ and Proton Exchange Between H₃⁺ and H₂, *The Journal of Physical Chemistry A* **119**, 12109 (2015).
- [42] G. Simons, R. G. Parr, and J. M. Finlan, New alternative to the dunham potential for diatomic molecules, *The Journal of Chemical Physics* **59**, 3229 (1973).
- [43] J. Zúñiga, J. A. G. Picón, A. Bastida, and A. Requena, On the use of optimal internal vibrational coordinates for symmetrical bent triatomic molecules, *The Journal of Chemical Physics* **122**, 224319 (2005).
- [44] I. W. Bulik, M. J. Frisch, and P. H. Vaccaro, Vibrational self-consistent field theory using optimized curvilinear coordinates, *The Journal of Chemical Physics* **147**, 044110 (2017).
- [45] R. Somma, G. Ortiz, E. Knill, and J. Gubernatis, Quantum simulations of physics problems (2003), arXiv:quant-ph/0304063.
- [46] D. Poulin and P. Wocjan, Sampling from the thermal quantum Gibbs state and evaluating partition functions with a quantum computer, *Physical Review Letters* **103**, 220502 (2009).
- [47] A. Riera, C. Gogolin, and J. Eisert, Thermalization in nature and on a quantum computer, *Phys. Rev. Lett.* **108**, 080402 (2012).
- [48] M. Motta, C. Sun, A. T. K. Tan, M. J. O’Rourke, E. Ye, A. J. Minnich, F. G. S. L. Brandão, and G. K.-L. Chan, Determining eigenstates and thermal states on a quantum computer using

- quantum imaginary time evolution, *Nature Physics* **16**, 205 (2019).
- [49] A. N. Chowdhury, G. H. Low, and N. Wiebe, A variational quantum algorithm for preparing quantum Gibbs states (2020), arXiv:2002.00055.
- [50] Y. Wang, G. Li, and X. Wang, Variational quantum Gibbs state preparation with a truncated Taylor series (2020), arXiv:2005.08797.
- [51] O. Higgott, D. Wang, and S. Brierley, Variational quantum computation of excited states, *Quantum* **3**, 156 (2019).
- [52] T. Jones, S. Endo, S. McArdle, X. Yuan, and S. C. Benjamin, Variational quantum algorithms for discovering Hamiltonian spectra, *Phys. Rev. A* **99**, 062304 (2019).
- [53] J. R. McClean, J. Romero, R. Babbush, and A. Aspuru-Guzik, The theory of variational hybrid quantum-classical algorithms, *New Journal of Physics* **18**, 023023 (2016).
- [54] L.-W. Wang and A. Zunger, Solving Schrödinger's equation around a desired energy: Application to silicon quantum dots, *The Journal of Chemical Physics* **100**, 2394 (1994).
- [55] K. Mitarai and K. Fujii, Methodology for replacing indirect measurements with direct measurements, *Phys. Rev. Research* **1**, 013006 (2019).
- [56] Y. Ibe, Y. O. Nakagawa, T. Yamamoto, K. Mitarai, Q. Gao, and T. Kobayashi, Calculating transition amplitudes by variational quantum eigensolvers (2020), arXiv:2002.11724.
- [57] F. Perakis, L. De Marco, A. Shalit, F. Tang, Z. R. Kann, T. D. Khne, R. Torre, M. Bonn, and Y. Nagata, Vibrational spectroscopy and dynamics of water, *Chemical Reviews* **116**, 7590 (2016).
- [58] N. Penkov, N. Shvirst, V. Yashin, E. Fesenko, and E. Fesenko, Terahertz spectroscopy applied for investigation of water structure, *The Journal of Physical Chemistry B* **119**, 12664 (2015).
- [59] J. R. McClean, M. E. Kimchi-Schwartz, J. Carter, and W. A. de Jong, Hybrid quantum-classical hierarchy for mitigation of decoherence and determination of excited states, *Phys. Rev. A* **95**, 042308 (2017).
- [60] R. Santagati, J. Wang, A. A. Gentile, S. Paesani, N. Wiebe, J. R. McClean, S. Morley-Short, P. J. Shadbolt, D. Bonneau, J. W. Silverstone, D. P. Tew, X. Zhou, J. L. O'Brien, and M. G. Thompson, Witnessing eigenstates for quantum simulation of Hamiltonian spectra, *Science Advances* **4**, eaap9646 (2018).
- [61] D. S. Abrams and S. Lloyd, Quantum algorithm providing exponential speed increase for finding eigenvalues and eigenvectors, *Phys. Rev. Lett.* **83**, 5162 (1999).

- [62] D. Wecker, M. B. Hastings, N. Wiebe, B. K. Clark, C. Nayak, and M. Troyer, Solving strongly correlated electron models on a quantum computer, *Phys. Rev. A* **92**, 062318 (2015).
- [63] A. Roggero and J. Carlson, Dynamic linear response quantum algorithm, *Phys. Rev. C* **100**, 034610 (2019).
- [64] L. K. Grover, A fast quantum mechanical algorithm for database search, in *Proceedings of the twenty-eighth annual ACM symposium on Theory of computing - STOC 96* (ACM Press, 1996).
- [65] L. K. Grover, Quantum computers can search rapidly by using almost any transformation, *Phys. Rev. Lett.* **80**, 4329 (1998).
- [66] A. M. Childs, D. Maslov, Y. Nam, N. J. Ross, and Y. Su, Toward the first quantum simulation with quantum speedup, *Proceedings of the National Academy of Sciences* **115**, 9456 (2018).
- [67] R. C. Fortenberry, X. Huang, A. Yachmenev, W. Thiel, and T. J. Lee, On the use of quartic force fields in variational calculations, *Chemical Physics Letters* **574**, 1 (2013).
- [68] E. L. Sibert, Modeling vibrational anharmonicity in infrared spectra of high frequency vibrations of polyatomic molecules, *The Journal of Chemical Physics* **150**, 090901 (2019).
- [69] R. Babbush, N. Wiebe, J. McClean, J. McClain, H. Neven, and G. K.-L. Chan, Low-depth quantum simulation of materials, *Phys. Rev. X* **8**, 011044 (2018).
- [70] R. Babbush, C. Gidney, D. W. Berry, N. Wiebe, J. McClean, A. Paler, A. Fowler, and H. Neven, Encoding electronic spectra in quantum circuits with linear T complexity, *Phys. Rev. X* **8**, 041015 (2018).
- [71] D. W. Berry, C. Gidney, M. Motta, J. R. McClean, and R. Babbush, Qubitization of arbitrary basis quantum chemistry leveraging sparsity and low rank factorization, *Quantum* **3**, 208 (2019).
- [72] V. von Burg, G. H. Low, T. Hner, D. S. Steiger, M. Reiher, M. Roetteler, and M. Troyer, Quantum computing enhanced computational catalysis (2020), arXiv:2007.14460.
- [73] M. Reiher, N. Wiebe, K. M. Svore, D. Wecker, and M. Troyer, Elucidating reaction mechanisms on quantum computers, *Proceedings of the National Academy of Sciences* **114**, 7555 (2017).
- [74] Z. Li, J. Li, N. S. Dattani, C. J. Umrigar, and G. K.-L. Chan, The electronic complexity of the ground-state of the fmo cofactor of nitrogenase as relevant to quantum simulations (2018), arXiv:1809.10307.
- [75] P. Jordan and E. Wigner, Uber das Paulische aquivalenzverbot, *Zeitschrift fur Physik* **47**, 631

- (1928).
- [76] S. B. Bravyi and A. Y. Kitaev, Fermionic quantum computation, *Annals of Physics* **298**, 210 (2002).
- [77] S. McArdle, T. Jones, S. Endo, Y. Li, S. C. Benjamin, and X. Yuan, Variational ansatz-based quantum simulation of imaginary time evolution, *npj Quantum Information* **5**, 75 (2019).
- [78] K.-S. Lee and U. R. Fischer, Truncated many-body dynamics of interacting bosons: A variational principle with error monitoring, *International Journal of Modern Physics B* **28**, 1550021 (2014).
- [79] M. P. Woods, M. Cramer, and M. B. Plenio, Simulating bosonic baths with error bars, *Phys. Rev. Lett.* **115**, 130401 (2015).
- [80] A. Kitaev, Quantum computations: algorithms and error correction, *Russian Mathematical Surveys* **52**, 1191 (1997).
- [81] T. Helgaker, P. Jorgensen, and J. Olsen, *Molecular Electronic-Structure Theory* (Wiley, 2013).
- [82] J. McClean, N. Rubin, K. Sung, I. D. Kivlichan, X. Bonet-Monroig, Y. Cao, C. Dai, E. S. Fried, C. Gidney, B. Gimby, P. Gokhale, T. Haner, T. Hardikar, V. Havlek, O. Higgott, C. Huang, J. Izaac, Z. Jiang, X. Liu, S. McArdle, M. Neeley, T. O'Brien, B. O'Gorman, I. Ozfidan, M. D. Radin, J. Romero, N. P. D. Sawaya, B. Senjean, K. Setia, S. Sim, D. S. Steiger, M. Steudtner, Q. Sun, W. Sun, D. Wang, F. Zhang, and R. Babbush, Openfermion: The electronic structure package for quantum computers, *Quantum Science and Technology* (2020).
- [83] R. M. Parrish, L. A. Burns, D. G. A. Smith, A. C. Simmonett, A. E. DePrince, E. G. Hohenstein, U. Bozkaya, A. Y. Sokolov, R. Di Remigio, R. M. Richard, J. F. Gonthier, A. M. James, H. R. McAlexander, A. Kumar, M. Saitow, X. Wang, B. P. Pritchard, P. Verma, H. F. Schaefer, K. Patkowski, R. A. King, E. F. Valeev, F. A. Evangelista, J. M. Turney, T. D. Crawford, and C. D. Sherrill, Psi4 1.1: An open-source electronic structure program emphasizing automation, advanced libraries, and interoperability, *Journal of Chemical Theory and Computation* **13**, 3185 (2017).
- [84] D. A. Matthews, L. Cheng, M. E. Harding, F. Lipparini, S. Stopkowicz, T.-C. Jagau, P. G. Szalay, J. Gauss, and J. F. Stanton, Coupled-cluster techniques for computational chemistry: The CFOUR program package, *The Journal of Chemical Physics* **152**, 214108 (2020).
- [85] A. Barbe, C. Secroun, and P. Jouve, Infrared spectra of 16O3 and 18O3: Darling and Dennison resonance and anharmonic potential function of ozone, *Journal of Molecular Spectroscopy* **49**,

171 (1974).

- [86] S. M. Adler-Golden, S. R. Langhoff, C. W. Bauschlicher, and G. D. Carney, Theoretical calculation of ozone vibrational infrared intensities, *The Journal of Chemical Physics* **83**, 255 (1985).
- [87] V. Havlíček, A. D. Córcoles, K. Temme, A. W. Harrow, A. Kandala, J. M. Chow, and J. M. Gambetta, Supervised learning with quantum-enhanced feature spaces, *Nature* **567**, 209 (2019).
- [88] H. Buhrman, R. Cleve, J. Watrous, and R. de Wolf, Quantum fingerprinting, *Phys. Rev. Lett.* **87**, 167902 (2001).
- [89] J. C. Garcia-Escartin and P. Chamorro-Posada, SWAP test and Hong-Ou-Mandel effect are equivalent, *Phys. Rev. A* **87**, 052330 (2013).
- [90] M. A. Nielsen and I. L. Chuang, *Quantum Computation and Quantum Information: 10th Anniversary Edition*, 10th ed. (Cambridge University Press, New York, NY, USA, 2011).
- [91] P. Virtanen, R. Gommers, T. E. Oliphant, M. Haberland, T. Reddy, D. Cournapeau, E. Burovski, P. Peterson, W. Weckesser, J. Bright, S. J. van der Walt, M. Brett, J. Wilson, K. Jarrod Millman, N. Mayorov, A. R. J. Nelson, E. Jones, R. Kern, E. Larson, C. Carey, Í. Polat, Y. Feng, E. W. Moore, J. Vand erPlas, D. Laxalde, J. Perktold, R. Cimrman, I. Henriksen, E. A. Quintero, C. R. Harris, A. M. Archibald, A. H. Ribeiro, F. Pedregosa, P. van Mulbregt, and Contributors, SciPy 1.0: Fundamental Algorithms for Scientific Computing in Python, *Nature Methods* **17**, 261 (2020).